

1 **Review 1**

2 **General comments**

3 The effect of non-water saturated sediments and that of groundwater quality needs to be stated more
4 explicit. I would think that there is data available from watersamples, well-logging or any other
5 information, that provides information about the height of the watertable and confirms that the
6 groundwater is fresh, and as such not a major factor in the resistivity.

7 *Actually, the effect of saturation is quite substantial and we have added a detailed comment on this in
8 the discussion. As long as the water saturated sand formation resistivity is higher than that of a "clay"-
9 formation our basic assumption is not violated and the translator function will, ideally, adjust
10 accordingly. In the specific case the pore water resistivity is sufficiently high that the clay layers are still
11 the most conductive.*

12 **Specific comments**

13 There are some issues in the paper I do not understand / are not clarified satisfactorily. One of the main
14 issues is scale. The translator function is defined on a 1km grid and then applied to boreholes in order to
15 obtain consistency between clay fraction from the lithology log and clay fraction from the resistivity
16 models, Fig. 1 and 2.

17 On page 1468, the authors mention the procedure to define the translator function at the resistivity
18 models, but the effects of the large distance between grid-node of the translator model and the
19 resistivity models is not discussed.

20 The final model has a grid size of 100m x 100m, which is considerable more detailed than the translator
21 model. The consequences of this difference in scale should be discussed.

22 *We have added a detailed discussion on these relevant issues in the 'discussion' section. The scale of the
23 translator function is defined by the 'scale' of changes in the resistivity-clay translation, and these are
24 generally thought to be slow. The resistivity data are used to described the actual positioning of clay and
25 sand units in the entire volume regardless of the translation, and it therefore make sense to have a
26 much denser grid here.*

27 Besides that, the consistency comparison between clay fraction from the resistivity models and from the
28 lithology logs (Fig. 1) involve some decisions about which borehole to use for the comparison. For
29 example, is there a distance constraint used for comparing boreholes with nearest resistivity model?

30 *I believe this is a misunderstanding of the concept. There is no such thing as 'a closest resistivity model'.
31 The comparison is done in the borehole positions based on values kriged from the resistivity positions.
32 This is done exactly to avoid having to discuss direction, search radius etc. There is of course an effective
33 search radius, but it is chosen so big (500 m) that several geophysical models contribute for most
34 boreholes.*

35 On page 1468, lines 14-18, the migration of the translator function to areas with few / no boreholes
36 needs justification. The decision to do this is rather crucial for the resulting model and at least an
37 attempt should be made to estimate the effects.

38 We agree that the choice of constraint strengths is important for the outcome. Setting the constraints
39 very loose we would be able to (over-)fit most boreholes, but it would at the price of an unrealistic
40 looking model. As we have no 'true model' to compare against the evaluation is done based on the
41 classical balance between fitting the data while having a reasonable model. These evaluations are
42 primarily based on visual evaluations comparing the results against key boreholes. A clarifying sentence
43 have been added in the 'Methodology' section and detailed paragraphs are also added to the
44 'Discussion'.

45 Page 1468, lines 19-23, the procedure is explained for obtaining the clay-fraction from the resistivity
46 model at the location of the borehole. Point kriging is used, and I would recommend that the authors
47 make clear that this is carried out with keeping in mind the maximum correlation distance. Beyond that
48 distance, the interpolation is merely a local averaging.

49 This is absolutely correct, but we find that this is going into too much detail, as we have references to
50 the kriging method itself. If the reader is unfamiliar with kriging many other aspects would require a
51 deeper discussion to be fulfilling.

52 The results, as displayed in Fig 6 and 7 are promising. It seems to confirm the general geology of the
53 area, but there is no rigorous validation of the procedure, e.g. performing cross-validation (leaving
54 boreholes out of the dataset, one by one, and comparing the estimate with the borehole data) to judge
55 the performance. Another option would be to split the dataset (e.g. 20%-80%) and estimate the quality
56 of the procedure on using 80% of the data on the remaining 20%. This would give the reader a better
57 "feel" of the quality of the results.

58 I see the point, but I think that the reader would only be more confused. Though, we did not even report
59 the data fit of the inversion result, which should have been there and we have added it now. The data fit
60 is a significant number saying if the data (boreholes) can be fitted by the model suggested by the
61 inversion process. It seems to me that the suggested approach requires that the boreholes are looked at
62 as "hard information", which is contrary to the approach here assigning actual noise to the borehole
63 descriptions. Also, given that the optimization is handled as an inversion problem removing parts of the
64 data set does not make much sense in my opinion. We would get data fits at the removed data points a
65 little worse than what we report here (1.26 – just outside the assigned noise), but how should that then
66 be interpreted? It is similar to taking a schlumberger sounding (VES) and removing some data points and
67 see if you can back-fit them with the remaining data. You can do that, but the fit would be a little poorer
68 than having all the data. If you remove the insignificant data the effect would be small; if you remove
69 crucial data the result would be worse. I am confident the result would be the same here – removing
70 one borehole at a time we would see that the remaining boreholes would produce an almost equally
71 good fit at the position of the missing borehole. A little bit worse as suggested by inversion theory, and
72 we would not have learned much.

73 The results are defined in terms of clay-fraction: the fraction of the length of an interval that is clay. How
74 would this convert to hydrological parameters?

75 *More comments on this issue have been added to this, but is also on purpose not to dive too deep into*
76 *this discussion as we are really trying to be general about the conceptual idea and not link it too tightly*
77 *to a specific use (even though the hydrological modelling is obvious...)*

78 The authors mention that, after clustering, the Norsminde are can be divided into sub-areas, with
79 different hydrological parameters. Is there a way to use the results of the clay-fraction model directly
80 into groundwater models?

81 *See above*

82 **1 Detailed comments (annotations in PDF-document)**

Page, Line	Review remarks	Authors response
1462,26	What does this mean in the context of 3D mapping?	Rephrased
1463,8	layers = surfaces; so what do you mean?	Corrected
1463,24	not proper English	Rephrased
1463,25	what is meant by geostatistical properties?	Rephrased
1463,26	explain what is meant by hard and soft data. Does not occur in the manuscript after this	Rephrased
1464,5-8	What do you want to say? It is not clear what this sentence means.	We have rephrased this sentence
1465,1	c or k?	K-mean (type-setting error "K" should not be italic)
1465,16	Add "Established"	Sentence rephrased.
1465,21	In Fig. 1, the resistivity models are not listed as data, but it is data, isn't it?	From and inversion point of view the resistivity models are not "data" in the concept. The data (observed data) that are fitted during the inversion are CF-data of the boreholes. The resistivity models is a part of the forward response (forward data) as described in section 2.2. The labels in fig. 1 is therefore correct.
1466, 27	statistical variance is denoted as σ^2 , σ = standard deviation	Agree. Corrected throughout the paper incl. in formulas.
1467, 7	sediment?	No change, we believe it is clear as it is.
1467, 20	Not all parameters are described / explained: K, rho	K is defined in equation 1., but we have clarified the text.
1468, 7	reference not very satisfactory: in review	Agree, but ... The referenced paper is in print (proofread recently), and there is no good alternative reference.

1468, 11	horizontal discretization? 1km?	Rephrased: "The horizontal discretization is typically 500-1000 m and a 2D bilinear horizontal interpolation of ..."
1468, 18	This is a rather tricky business, migrating to areas without supporting data. You need to justify this!	It is true that it is tricky business to setup constraints that migrate information to less data dense areas. Here, it is merely a statement on how the inversion works, but we added a short extra sentence and addressed the question in more general terms in the discussion section.
	Kriging is not taken the spatial variance into account but uses the spatial correlation (as captured in the variogram) to estimate spatial interpolation variance. Except, when you mean that you are using "kriging with uncertain data", in that case it should be stated explicitly. You probably mean the spatial variation	"kriging with uncertain data" is used in this case. Paragraph is rephrased to make it clear.
1468, 18	How? See previous remark!	We believe this is covered by the stated reference for the used kriging code (Pebesma and Wesseling, 1998)
1469, 14-15	is this the standard deviation of the variance?. this means the standard deviation!	Corrected, see also authors response 1466, 27
1472, 14	superfluous remark	Removed
1472, 18	length?	Corrected to "calculation intervals" to be consistent with the concept explanation in section 2
1472, 28	you mean the vertical density?	Yes. Corrected to "Vertical sample density"
1473, 7	are often drilled for the purpose of	Rephrased
1474, 23	Are this factors that are in line with other studies / experiences? They do not mean anything to me	Paragraph extended and rephrased to add some qualitative statements Comment: Since the constrains are specified directly on the translator model parameters there is nothing to compare with as this is the first time the concept is presented.
1474, 27	sentence is not correct: "through subsequent test-inversions"	Corrected
1475, 7	I do not understand this! what does "are included" mean?	The sentence have been rephrased and extended substantially.
1475, 9	How do you obtain this 100m model? Your input is the resistivity models, converetd to clay fraction, I assume. Some kind of interpolation? Which technique?	Valid point - the explanation is heavily extended on this part.
1475, 21	Of course these are smooth, because they originate from a 1km grid	Rephrased for clarity

1476, 8	What is the height of the water-table in the area?	This is relevant, but the whole idea is to address many different issues with one parameter. More justification has been added in the introduction and in particular in the discussion.
1476, 9	This is quite troublesome, since this would also have an effect on all previous calculations! What is known about the groundwater quality / salinity?	This issue is now elaborated in the Discussion section. Regarding salinity: Saltwater intrusion is not a of major concern for the Norsminde area since the clay sequence extends almost to the surface in the coastal area.
1476, 18	What do you mean by "correct" ?	Rephrased
1476, 22	With	Corrected
1476, 27	Although you will have layers that cross the discretisation interval, with part in one interval and part in the lower lying interval. This also causes non-binary intervals.	Rephrased for clarity
1477, 9	Well., this is only one section and a visual inspection of the results. I would like to see a more rigorous comparison, e.g. cross-validation, see general comments.	See comment under general comments above
1477, 27	insert: "are able to"	Corrected
1481, 21	Replication	Corrected
Fig.1	resistivity model is also data?	See 1465,21
Fig.2	What is the spatial lay-out of the resistivity models, compared to this layout of the translator function? Gives an idea of the scale differences	Fig. 2 is a principle sketch for the translator function grid and constraints. For the Case story the layout of the EM-survey/resistivity model is described in section 3.2. The setup of the translator function grid for the case story is specified in section 3.3 and the horizontal node discretization can be see e.g. in fig. 7a.
Fig.7	How come there is a CF model while there is no resistivity?	See 1475, 7
Fig. 7	First time you mention that resistivity is interpolated	It is only for presenting a resistivity slice that the resistivity value has been interpolated. The CF-concept do not use interpolated resistivities as input as described in section 2.2. Fig. label updated to: "Resistivity slice (interpolated)"

Fig.9	<p>Why not use relative frequency on the y-axis? No. of voxels is not very informative.</p> <p>And how does this compare to the borehole data? Is the frequency similar?</p>	<p>Y-axis: Agree. Figure axis change to "percent of voxels".</p> <p>1) The distribution of the borehole CF values are not really comparable with the resistivity CF-values distribution, since the sampling of the model space is heavily biased towards the near surface and non clay areas for the Boreholes. The drills are also typically ending when reaching the pre-Quaternary low resistivity "bottom" clay layer. 2) The borehole CF-values do not end up in a cluster!.</p>
-------	--	---

83

84 **Large scale 3D-modeling by integration of**
85 **resistivity models and borehole data**
86 **through inversion**

87

88 Authors: Nikolaj Foged¹, Pernille Aabye Marker², Anders Vest Christensen¹, Peter Bauer-Gottwein²,
89 Flemming Jørgensen³, Anne-Sophie Høyer³, Esben Auken¹

90 ¹HydroGeophysics Group, Department of Geoscience, Aarhus University, Denmark.

91 ²Department of Environmental Engineering, Technical University of Denmark

92 ³Geological Survey of Denmark and Greenland

93 **ABSTRACT**

94 We present an automatic method for parameterization of a 3D model of the subsurface, integrating
95 lithological information from boreholes with resistivity models through an inverse optimization, with the
96 objective of further detailing for geological models or as direct input to groundwater models. The
97 parameter of interest is the clay fraction, expressed as the relative length of clay-units in a depth interval.
98 The clay fraction is obtained from lithological logs and the clay fraction from the resistivity is obtained
99 by establishing a simple petrophysical relationship, a translator function, between resistivity and the clay
100 fraction. Through inversion we use the lithological data and the resistivity data to determine the optimum
101 spatially distributed translator function. Applying the translator function we get a 3D clay fraction model,

102 which holds information from the resistivity dataset and the borehole dataset in one variable. Finally, we
103 use k-means clustering to generate a 3D model of the subsurface structures. We apply the concept to the
104 Norsminde survey in Denmark integrating approximately 700 boreholes and more than 100,000
105 resistivity models from an airborne survey in the parameterization of the 3D model covering 156 km².
106 The final five-cluster 3D model differentiates between clay materials and different high resistive materials
107 from information held in resistivity model and borehole observations respectively.

108 2 INTRODUCTION

109 In a large-scale geological and hydrogeological modeling context, borehole data seldom provide an
110 adequate data base due to low spatial density in relation to the complexity of the subsurface to be mapped.
111 Contrary, dense areal coverage can be obtained from geophysical measurements, and particularly airborne
112 EM methods are suitable for 3D mapping, as they cover large areas in a short period of time. However,
113 the geological and hydrogeological parameters are only mapped indirectly, and interpretation of the
114 airborne results is needed, which is often based on site-specific relationships. Linking electrical
115 resistivity to hydrological properties is therefore an area of increased interest as reviewed by Slater
116 (2007).

Deleted: Therefore e.g. the link

Deleted: between

Deleted: and electrical properties has

Deleted: been

117 Integrating geophysical models and borehole information has proved to be a powerful combination for 3D
118 geological mapping (Jørgensen et al., 2012; Sandersen et al., 2009) and several modeling approaches
119 have been reported. One way of building 3D-models is through a knowledge-driven (cognitive), manual
120 approach (Jørgensen et al., 2013a). This can be carried out by making layer-cake models composed of
121 stacked layers or by making models composed of structured or unstructured 3D meshes where each voxel
122 is assigned a geological/hydrogeological property. The latter allows for a higher degree of model
123 complexity to be incorporated (Turner, 2006; Jørgensen et al., 2013a). The cognitive approach enables
124 various types of background knowledge such as the sedimentary processes, sequence stratigraphy, etc. to
125 be utilized. However, the cognitive modeling approach is difficult to document and reproduce due to its
126 subjective nature. Moreover, any cognitive approach will be quite time-consuming, especially when
127 incorporating large airborne electromagnetic (AEM) surveys, easily exceeding 100,000 resistivity models.

Deleted: separated by surfaces

128 Geostatistical modeling approaches such as multiple-point geostatistical methods (Daly and Caers, 2010;
129 Strebelle, 2002), transition probability indicator simulation (Fogg, 1996) or sequential indicator
130 simulation (Deutsch and Journel, 1998), provide models with a higher degree of objectivity in shorter
131 time compared to the cognitive, manual modeling approaches. An example of combining AEM and
132 borehole information in a transition probability indicator simulation approach is given by He et al. (2014).
133 Geostatistical modeling approaches based primarily on borehole data often faces the problem that the data

Deleted: He et al.

Deleted: 2013

Deleted: The use of only borehole data in g

Deleted: problems

144 are too sparse to represent the lateral heterogeneity [at the desired spatial scale](#). Including geophysical data
145 enables a more accurate estimation of [the geostatistical properties especially laterally](#). ~~This could be~~
146 ~~determination of the transition probabilities and the mean lengths of the different units. Though, the~~
147 ~~geophysical data also~~ opens the question [to what degree the different data types should be honored](#) in the
148 model simulations and estimations. Combined use of geostatistical and cognitive approaches can be a
149 suitable solution in some cases ([Jørgensen et al., 2013b](#); Raiber et al., 2012; Stafleu et al., 2011).
150 Integration of borehole information and geological knowledge as prior information directly in the
151 inversion of the geophysical data is another technique to combine the two types of information and
152 thereby achieve better geophysical models and subsequently better geological and hydrological models
153 (~~Høyer et al., 2014~~; Wisén et al., 2005).

Deleted: especially laterally

Deleted: ,

Deleted: but

Deleted: of what to use as *hard* and *soft* data

Deleted: Jørgensen et al., 2013b

Deleted: Høyer et al., 2014

154 Geological models are commonly used as the basis for hydrostratigraphical input to groundwater models.
155 ~~However, even though groundwater model predictions are sensitive to variations in the hydrostratigraphy~~
156 ~~the groundwater model calibration is non-unique and different hydrostratigraphic models may produce~~
157 ~~similar results~~ (Seifert et al., 2012).

Deleted: While m

Deleted: y, non-uniqueness with respect to hydrostratigraphy is inherent to groundwater models

158 Sequential, joint and coupled hydrogeophysical inversion techniques (Hinnell et al., 2010) have been used
159 to inform groundwater models with both geophysical and traditional hydrogeological observations. Such
160 techniques use petrophysical relationships to translate between geophysical and hydrogeological
161 parameter spaces. For applications in groundwater modeling using electromagnetic data see e.g Dam and
162 Christensen (2003) and Herckenrath et al. (2013). Also clustering analyses can be used to delineate
163 subsurface hydrogeological properties. Fuzzy c-means clustering has been used to delineate geological
164 features from measured EM34 signals with varying penetration depths (Triantafilis and Buchanan, 2009)
165 and to delineate the porosity field from tomography inverted radar attenuation and velocities and seismic
166 velocities (Paasche et al., 2006).

167 We present an automatic method for parameterization of a 3D model of the subsurface. The geological
168 parameter we map is the clay fraction (CF), expressed as the cumulated thickness of *clay in a depth*
169 *interval relative to the interval length*. [In this paper we refer to clay as material described as clay in a](#)
170 [lithological well log regardless the type of clay; clay till, mica clay, Palaeogene clay, etc. This term is](#)
171 [robust in the sense that most geologists and drillers have a common conception on the description of clay](#)
172 [and it can easily be derived from the lithological log](#). The method integrates lithological information from
173 boreholes with resistivity information, typically from large-scale geophysical AEM surveys. We obtain
174 the CF from the resistivity data by establishing a petrophysical relationship, a translator function, between
175 resistivity and the CF. Through an inverse mathematical formulation we use the lithological borehole data
176 to determine the optimum parameters of the translator function. Hence, the 3D CF-model holds
177 information from the resistivity dataset and the borehole dataset in one variable. As a last step we cluster

Deleted: ¶

190 our model space represented by the CF-model and geophysical resistivity model using k-means clustering
191 to form a structural 3D cluster model with the objective of further detailing for geological models or as
192 direct input to groundwater models.

193 Lithological interpretation of a resistivity model is not trivial since the resistivity of a geological media is
194 controlled by: porosity, pore water conductivity, degree of saturation, amount of clay minerals, etc.
195 Different, primarily empirical models, try to explain the different phenomena, where Archie's law
196 (Archie, 1942) is the most fundamental empirical model taking the porosity, pore water conductivity and,
197 the degree of saturation into account, but does not account for electrical conduction of currents taking
198 place on the surface of the clay minerals. The Waxman and Smits model (Waxman and Smits, 1968)
199 together with the Dual Water model of Clavier et al. (1984) provides a fundamental basis for widely and
200 repeatedly used empirical rules for shaly sands and material containing clay (e.g. Bussian, 1983; Sen,
201 1987; Revil and Glover, 1998).

202 However, in a sedimentary depositional environment it can be assumed in general that clay or clay rich
203 sediments will exhibit lower resistivities than the non-clay sediments, silt, sand, gravel, and chalk. As
204 such, discrimination between clay and non-clay sediments based on resistivity models is feasible and the
205 CF-value is a suitable parameter to work with in the integration of resistivity models and lithological logs.
206 A 3D CF-model or clay/sand model will also contain key structural information for a groundwater model,
207 since it delineates the impermeable clay units and the permeable sand/gravel units.

208 With the CF-concept we use a two parameter resistivity to CF translator function which relies on the
209 lithological logs providing the local information for the optimum resistivity to CF-translation. Hence, we
210 avoid describing the physical parameters explaining the resistivity images explicitly.

211 First, we give an overall introduction to the CF-concept, and then we move to a more detailed description
212 of the different parts: observed data and uncertainty, forward modeling, inversion and minimization, and
213 clustering. Last we demonstrate the method in a field example with resistivity data from an airborne
214 SkyTEM survey combined with quality-rated borehole information.

215 **3 METHODOLOGY**

216 Conceptually, our approach sets up a function that best describes the petrophysical relationship between
217 clay fraction and resistivity. Through inversion we determine the optimum parameters of this translator
218 function, by minimizing the difference between the clay fraction calculated from the resistivity models
219 (Ψ_{res}) and the observed clay fraction in the lithological well logs (Ψ_{log}).

220 | [A key aspect in the concept is that the translator function can change horizontally and vertically adapting](#)
221 | [to the local conditions and borehole data. The calculation is carried out in](#) a number of elevation intervals
222 | (calculation intervals) [to cover an entire 3D model space. Having obtained the optimum](#) and spatially
223 | distributed translator function we can transform the resistivity models to form a 3D clay fraction model,
224 | incorporating the key information from both the resistivity models and the lithological logs into one
225 | parameter. The CF-concept is a further development to three dimensions of the accumulated clay
226 | thickness concept by [Christiansen et al., 2014](#), which is formulated in 2D.

Deleted: We do this for

Deleted: that are mutually constrained

Deleted:

Deleted: mized

Deleted: Christiansen et al., 2013

Deleted: Christiansen et al., 2014

227 | The flowchart in Figure 1 provides an overview of the CF-concept. The observed clay fraction (Ψ_{\log}) is
228 | calculated from the lithological logs (box 1) in the calculation intervals. The translator function (box 2)
229 | and the resistivity models (box 3) form the forward response which produces a resistivity-based clay
230 | fraction (box 4) in the different calculation intervals. The parameters of the translator function are
231 | updated during the inversion to obtain the best consistency between Ψ_{res} and Ψ_{\log} . The output is the
232 | optimum resistivity-to-clay fraction translator function (box 5) and when applying this to the resistivity
233 | models (the forward response of the final iteration), we obtain the optimum Ψ_{res} and block kriging is used
234 | to generate a regular 3D CF model (box 6).

235 | The final step is a k-means clustering analysis (box 7). With the clustering we achieve a 3D model of the
236 | subsurface delineating a predefined number of clusters that represent zones of similar physical properties,
237 | which can be used as input in, for example, a detailed geological model or as structural delineation for a
238 | groundwater model.

239 | The subsequent paragraphs detail the description of the individual parts of the concept.

240 | **3.1 Observed data - lithological logs and clay fraction**

241 | The common parameter derived from the lithological logs and resistivity datasets is the clay fraction
242 | (Figure 1, boxes 1-4). [The clay fraction, of a given depth interval in a borehole \(named \$\Psi_{\log}\$ \) is calculated](#)
243 | as the cumulative thickness of layers described as *clay* divided by the length of the interval. By using this
244 | definition of clay and clay fraction we can easily calculate Ψ_{\log} in depth intervals for any lithological well
245 | log [as the example in Figure 2a shows.](#) Having retrieved the Ψ_{\log} values we then need to estimate their
246 | uncertainties since a variance estimate, σ_{\log}^2 is needed in the evaluation of the misfit to Ψ_{res} .

Deleted: It is a common assumption that a petrophysical relationship between resistivity and clay content can be established shown for instance by Waxman and Smits (1968) and Shevlin et al. (2007). From the lithological logs we only have a lithological description, and in many cases only a very simple one; sand, clay, gravel, chalk, etc. Even in cases where more detailed descriptions with for instance sedimentary facies (e.g. clay till) or age (e.g. Palaeogene clay) are available, is it not possible to obtain the actual clay content from the descriptions. This is only possible if detailed lab-analyses have been carried out, which are extremely rare on a larger scale. In this paper we therefore refer to clay as material described as clay in a lithological well log regardless the type of clay; clay till, mica clay, Palaeogene clay, etc. This term is robust in the sense that most geologists and drillers have a common conception on the description of clay.

Deleted: Ψ_{\log} ,

Deleted: therefore

Deleted: the

Deleted: clay fraction

Deleted: The drilling method is one of the key parameters affecting the uncertainty of the well log data. ¶

247 | The drillings are conducted with a range of different methods. This has a large impact on the uncertainties
248 | of the lithological well log data. The drilling methods span from core drilling resulting in a very good
249 | base for the lithology classification, to direct circulation drillings (cuttings are flushed to the surface
250 | between the drill rod and the formation) resulting in poorly determined layer boundaries and a very high
251 | risk of getting [the](#) samples contaminated due to the travel time from the bottom to the surface. **Other**

288 parameters affecting the uncertainty of the Ψ_{log} are parameters like sample interval and density, accuracy
289 of the geographical positioning and elevation, and the credibility of the contractor.

Deleted: ,

290 3.2 Forward data – the translator function

291 For calculating the clay fraction for a resistivity model, Ψ_{res} , we use the translator function as shown in
292 Figure 2b which is defined by a m_{low} and a m_{up} parameter. m_{low} and m_{up} represents the clay and sand
293 cut-off values. So for resistivity values below m_{low} the layer is counted as clay ($W \approx 1$) and for resistivity
294 values above m_{up} the layer is counted as sand ($W \approx 0$). The translator function ($W(\rho)$) is mathematically a
295 scaled complementary error function, defined as:

Deleted: a simple two-parameter

Deleted: The translator function is described fully by

$$W(\rho) = 0.5 \cdot \operatorname{erfc}\left(\frac{K \cdot (2\rho - m_{up} - m_{low})}{(m_{up} - m_{low})}\right)$$

Deleted: ,

$$K = \operatorname{erfc}^{-1}(0.0025 \cdot 2)$$

296 (1)

297 where m_{low} and m_{up} are defined as the resistivity (ρ) at which the translator function, $W(\rho)$, returns a
298 weight of 0.975 and 0.025 respectively (the K -value scales the erfc function accordingly). For a layered
299 resistivity model, the Ψ_{res} for a single resistivity model value in one calculation interval, is then calculated
300 as:

Deleted: an

$$\Psi_{res} = \frac{1}{\sum t_i} \cdot \sum_{i=1}^N W(\rho_i) \cdot t_i$$

301 (2)

302 where N is the number of resistivity layers in the calculation interval, $W(\rho_i)$ is the clay weight for the
303 resistivity in layer i , t_i is the thickness of the resistivity layer, and $\sum t_i$ is the length of the calculation
304 interval. In other words, W weights the thickness a resistivity layer, so for a resistivity below m_{low} the
305 layer thickness is counted as clay ($W \approx 1$) while for a resistivity above m_{up} the layer is counted as non-
306 clay ($W \approx 0$). Figure 2a shows how a single resistivity model is translated into Ψ_{res} in a numbers of
307 calculation intervals.

Deleted:

308 The resistivity models are also associated with an uncertainty and if the variance estimates of the
309 resistivities and thicknesses for the geophysical models are available we take these into account. The

317 propagation of the uncertainty from the resistivity models to the Ψ_{res} values is described in detail in
318 [Christiansen et al. \(2014\)](#).

Deleted: Christiansen et al., 2013

Deleted: Christiansen et al.

Deleted: 2014

319 To allow for variation, laterally and vertically, in the resistivity to Ψ_{res} translation, a regular 3D grid is
320 defined for the survey block ([Figure 3](#)). Each grid node holds one set of m_{up} and m_{low} parameters. The
321 vertical discretization follows the clay fraction calculation intervals, typically [4-20 m increasing with](#)
322 [depth. The horizontal discretization is typically 0.5-2 km and a](#) 2D bilinear horizontal interpolation of the
323 m_{up} and m_{low} is applied to define the translator function uniquely at the positions of the resistivity models.

Deleted:

Deleted:

Deleted: 1

Deleted: intervals, A

Deleted: .

324 To migrate information of the translator function from regions with many boreholes to regions with few
325 boreholes or with no boreholes, horizontal and vertical smoothness constraints are applied between the
326 translator functions at each node point as shown in [Figure 3](#). [Choosing appropriate constraints is based on](#)
327 [the balance between fitting the data while having a reasonable model. The balance is site and data](#)
328 [specific, but would typically be based on visual evaluations comparing the results against key boreholes.](#)

329 The smoothness constraints furthermore act as regularization and stabilize the inversion scheme.

330 Finally, we [need to](#) estimate Ψ_{res} values at the Ψ_{log} positions (named Ψ_{res}^*) [for evaluation. We estimate the](#)
331 [\$\Psi_{res}^*\$ values by making a](#) point kriging interpolation [of the \$\Psi_{res}\$ values and associated uncertainties within](#)
332 [a search radius of typically 500 m.](#) The experimental semi-variogram is calculated from the Ψ_{res} values
333 for the given calculation interval and can normally be approximated well with an exponential function,
334 which then enters the kriging interpolation. The code Gstat (Pebesma and Wesseling, 1998) is used for
335 kriging, variogram calculation, and variogram fitting. [Hence, for the output estimates of the \$\Psi_{res}^*\$ both the](#)
336 original [variance](#) of Ψ_{res} and [the variance on the kriging interpolation itself is included to provide total](#)
337 [variance estimates of the \$\Psi_{res}^*\$ values \(\$\sigma_{res}^{2*}\$ \), which](#) are needed for a meaningful evaluation of the data
338 misfit at the borehole positions.

Deleted: using

Deleted: By using kriging for interpolation the spatial variance of Ψ_{res} is taken into account

Deleted: , and even more important, it provides uncertainty estimates (σ_{res}^*) of the Ψ_{res}^* values, which include

Deleted: uncertainty

Deleted: . These uncertainty estimates

339 3.3 Inversion - objective function and minimization

340 The inversion algorithm in its basic form consists of a nonlinear forward mapping of the model to the data
341 space:

$$\delta\Psi_{obs} = \mathbf{G}\delta\mathbf{m}_{true} + \mathbf{e}_{log}$$

(3)

343 where $\delta\Psi_{obs}$ denotes the difference between the observed data (Ψ_{log}) and the non-linear mapping of the
344 model to the data space (Ψ_{res}). $\delta\mathbf{m}_{true}$ represents the difference between the [model parameters \(\$m_{up}\$, \$m_{low}\$ \)](#)
345 [of the true, but unknown](#) translator function and an arbitrary reference model [\(the initial starting model](#)

Deleted:

364 | [for the first iteration, then at later iterations the model from the previous iteration](#)). e_{\log} is the
 365 | observational error, and G denotes the Jacobian matrix that contains the partial derivatives of the
 366 | mapping. The general solution to the non-linear inversion problem of equation (3) is described by
 367 | [Christiansen et al. \(2014\)](#) and is based on Auken and Christiansen (2004) and Auken et al. (2005).

368 | The objective function, Q , to be minimized includes a data term, R_{dat} , and a regularization term from the
 369 | horizontal and vertical constraints, R_{con} . R_{dat} is given as:

$$R_{\text{dat}} = \sqrt{\frac{1}{N_{\text{dat}}} \cdot \sum_{i=1}^{N_{\text{dat}}} \frac{(\Psi_{\log,i} - \Psi_{\text{res},i}^*)^2}{\sigma_i^2}}$$

370 | (4)

371 | where N_{dat} is the number of Ψ_{\log} values and σ_i^2 is the combined variance of the i 'th Ψ_{\log} (σ_{\log}^2) and Ψ_{res}
 372 | (σ_{res}^{2*}) given as:

$$\sigma_i^2 = \sigma_{\log,i}^2 + \sigma_{\text{res},i}^{2*}$$

373 | (5)

374 | The inversion is performed in logarithmic model space to prevent negative parameters, and R_{con} is
 375 | therefore defined as:

$$R_{\text{con}} = \sqrt{\frac{1}{N_{\text{con}}} \cdot \sum_{i=1}^{N_{\text{con}}} \frac{(\ln(m_j) - \ln(m_k))^2}{(\ln(e_{r,i}))^2}}$$

376 | (6)

377 | Where e_r is the regularizing constraint between the two constrained parameters m_j and m_k of the translator
 378 | function and N_{con} is the number constraint pairs. The e_r values in equation (6) are stated as constraint
 379 | factors, meaning that an e_r factor of 1.2 corresponds approximately to a model change of +/- 20%.

380 | In total the objective function Q becomes:

381

$$Q = \sqrt{\frac{N_{\text{dat}} \cdot R_{\text{dat}}^2 + N_{\text{con}} \cdot R_{\text{con}}^2}{(N_{\text{dat}} + N_{\text{con}})}}$$

Deleted: Christiansen et al. (2013)

Deleted: Christiansen et al.

Deleted: 2014

Deleted: $(\sigma_i)^2$

Deleted: σ_i

Deleted: $\sqrt{\sigma_{\log,i}^2 + \sigma_{\text{res},i}^{2*}}$

388 (7)

389 Furthermore, is it possible to add prior information as a prior constraint on the parameters of the translator
390 function, which just adds a third component to Q in equation (7) similar to R_{con} in equation (6).

391 The minimization of the non-linear problem is performed in a least squares sense by using an iterative
392 Gauss-Newton minimization scheme with a Marquardt modification. The full set of inversion equations
393 and solutions are presented in [Christiansen et al. \(2014\)](#).

394 3.4 Cluster analysis

395 The delineation of the 3D model is obtained through a k-means clustering analysis which distinguishes
396 groups of common properties within multivariate data. We have based the clustering analysis on the CF-
397 model and the resistivity model. Other data, which are informative for structural delineation of geological
398 or hydrological properties, can also be included in the cluster analysis. For example this could be
399 geological a priori information or groundwater quality data. The resistivity model is part of the CF-model,
400 but is reused for the clustering analysis because the representation of lithology used in the CF-model
401 inversion has simplified the geological heterogeneity captured in the resistivity model.

402 K-means clustering is a hard clustering algorithm used to group multivariate data. A k-means cluster
403 analysis is iterative optimization with the objective to minimize a distance function between data points
404 and a predefined number of clusters (Wu, 2012). We have used Euclidean length as a measure of
405 distance. We use the k-means algorithm in MATLAB R2013a, which has implemented a two-phase
406 search, batch and sequential, to minimize the risk of reaching a local minimum (Wu, 2012). K-means
407 clustering can be performed on several variables, but for variables to impact the clustering equally, data
408 must be standardized and uncorrelated. The CF-model and resistivity model are by definition correlated.
409 We use Principal Component Analysis (PCA) to obtain uncorrelated variables.

410 Principal component analysis is a statistical analysis based on data variance formulated by Hotelling
411 (1933). The aim of a PCA is to find linear combinations of original data while obtaining maximum
412 variance of the linear combinations (Härdle and Simar, 2012). This results in an orthogonal
413 transformation of the original multi-dimensional variables into a space where dimension one has largest
414 variance, dimension two has second largest variance, etc. In this case the PCA is not used to reduce
415 variable space, but only to obtain an orthogonal representation of the original variable space to use in the
416 clustering analysis. Principal components are orthogonal and thus uncorrelated, which makes the
417 principal components useful in the subsequent clustering analysis. The PCA is scale sensitive and the
418 original variables must therefore be standardized prior to the analysis. Because the principal components

Deleted: Christiansen et al.(2013)

Deleted: Christiansen et al.

Deleted: 2014

Deleted: .

423 have no physical meaning a weighting of the CF-model and the resistivity model cannot be included in
424 the k-means clustering. Instead the variables are weighed prior to the PCA.

425 **4 NORSMINDE CASE**

426 The Norsminde case model area is located in eastern Jutland, Denmark (Figure 4) around the town of
427 Odder (Figure 5) and covers 156 km², representing the Norsminde Fjord catchment. The catchment area
428 has been mapped and studied intensely in the NiCA research project in connection to nitrate reduction in
429 geologically heterogeneous catchments (Refsgaard et al., 2014). The modeling area has a high degree of
430 geological complexity in the upper part of the section. The area is characterized by Palaeogene and
431 Neogene sediments covered by glacial Pleistocene deposits. The Palaeogene is composed of fine-grained
432 marl and clay and the Neogene layers consist of marine Miocene clay interbedded with deltaic sand layers
433 (Rasmussen et al. 2010). The Neogene is not present in the southern and eastern part of the area where the
434 glacial sediments therefore directly overlie the Palaeogene clay. The Palaeogene and Neogene layers in
435 the region are frequently incised by Pleistocene buried tunnel valleys and one of these is present in the
436 southern part, where it crosses the model area to great depths with an overall E-W orientation (Jørgensen
437 and Sandersen, 2006). The Pleistocene deposits generally appear very heterogeneous and according to
438 boreholes they are composed of glacial meltwater sediments and till.

439 **4.1 Borehole data**

440 In Denmark, the borehole data are stored in the national database Jupiter (Møller et al., 2009) dating back
441 to 1926 as an archive for all data and information obtained by drilling. Today, the Jupiter database holds
442 information about more than 240,000 boreholes. For the lithological logs a fixed lithology code list is
443 available and the different types of clay layers are easily identified, and the Ψ_{\log} values for the
444 calculation intervals can be calculated.

445 For the model area, approximately 700 boreholes are stored in the database. Based on borehole meta-data
446 found in the database we use an automatic quality rating system, where each borehole is rated from 1-4
447 (He et al., 2014). The ratings are used to apply the lithological logs with uncertainty (weights) used in the
448 inversion.

449 The meta-data used for the quality-rating are:

- 450 • Drill method: auger, direct circulation, air-lift drilling, etc.
- 451 • Vertical sample density
- 452 • Accuracy of the geographical position: GPS or manual map location

Deleted: Similar databases are maintained in other countries.

Deleted: all

Deleted: desired elevation intervals

Deleted: He et al., 2013

Deleted: S

- 459
- Accuracy of the elevation: Differential GPS or other
- 460
- Drilling purpose: scientific, water abstraction, geophysical shot holes, etc.
- 461
- Credibility of drilling contractor

462 The boreholes are **awarded** points in the different categories and finally grouped into four quality groups
463 according to their total score. Boreholes in the lowest quality group (4) are primarily boreholes with low
464 sample frequencies (less than 1 sample per 10 m), low accuracy in geographical position, and/or drilled
465 as geophysical shot holes for seismic exploration.

466 The locations, quality ratings and drill depths of the boreholes are shown in Figure 5b. The drill depths
467 and quality ratings are summarized in Figure 6. As the top bar in Figure 6 shows, 4 % of the boreholes are
468 categorized as quality 1, 46 % as quality 2, 32 % as quality 3, and 18 % as quality 4. The uncertainties of
469 the Ψ_{\log} values for the quality groups 1-4 are based on a subjective evaluation and are defined as 10%,
470 20%, 30%, and 50%, respectively. The number of boreholes drastically decreases with depth as shown in
471 Figure 6. Thus, while about 100 boreholes are present in a depth of 60 m, only 25 boreholes reach a depth
472 greater than 90 m.

Deleted: and

Deleted: , while the

Deleted: t

473 4.2 EM data

474 The major part of the model area is covered by SkyTEM data and adjoining ground based TEM
475 soundings are included in the resistivity dataset (Figure 5a).

476 The SkyTEM data were collected with the newly developed SkyTEM¹⁰¹ system (Schamper et al., 2013).
477 The SkyTEM¹⁰¹ system has the ability to measure very early times, which improves the resolution of the
478 near surface geological layers when careful system calibration and advanced processing and inversion
479 methodologies are applied (Schamper et al., 2014). The recorded times span the interval from ~3 μ s to 1-
480 2 ms after end of the turn-off ramp, which gives a depth of investigation (Christiansen and Auken, 2012)
481 of approximately 100 m for an average ground resistivity of 50 Ω m. The SkyTEM survey was performed
482 with a dense line spacing of 50 m for the western part and 100 m line spacing for eastern part (Figure 5a).
483 Additional cross lines were made in a smaller area, which brings the total up to approximately 2000 line
484 km. The sounding spacing along the lines is approximately 15 m resulting in a total of 106,770 1D
485 resistivity models. The inversion was carried out in a spatially constrained inversion setup (Viezzoli et al.,
486 2008) with a smooth 1D-model formulation (29 layers, with fixed layer boundaries), using the AarhusInv
487 inversion code (Auken et al., 2014) and the Aarhus Workbench software package (Auken et al., 2009) .
488 The resistivity models have been terminated individually at the estimated depth of investigation (DOI)
489 calculated as described by Christiansen and Auken (2012).

493 The ground based TEM soundings originate from mapping campaigns in the mid-1990s. The TEM
494 sounding were all acquired with the Geonics TEM47/PROTEM system (Geonics Limited) in a central
495 loop configuration with a 40 by 40 m² transmitter loop. Data were inverted single site using a 1D layered
496 resistivity model with 3 to 5 layers depending on the number of layers needed to fit the data.

497 4.3 Model setup

498 The 3D translator function grid has a horizontal discretization of 1 km, with 16 nodes in the x-direction
499 and 18 nodes in the y-direction. Vertically the model spans from 100 masl (highest surface elevation) to
500 120 mbsl. The vertical discretization is 4 m above sea level and 8 m below sea level, which results in 40
501 calculation intervals. Hence, in total the model grid holds 16x18x40=11,520 translator functions each
502 holding two parameters. Translator functions in the 3D grid situated above terrain, below DOI of the
503 resistivity models, and outside geophysical coverage does not contribute at all, and are only included to
504 make the translator function grid regular for easier computation/bookkeeping. The effective number of
505 translator functions, is therefore close to 5,200.

Deleted: Node points in the t

506 The regularization constraints between neighboring translator model nodes are set relatively loose to
507 promote a predominantly data driven inversion problem. In this case we uses horizontal constraint factors
508 of 2 and vertical constraint factors of 3. This roughly corresponds to allowed translator parameter
509 variations of a factor of 2 (horizontal) and a factor of 3 (vertical) relative to adjacent translator
510 parameters. The resulting variations in the translator models grid is a trade-off between data, data
511 uncertainties and the constraints (equation (7)). A spatially uniform initial translator function was used
512 with $m_{low} = 35 \Omega m$ and $m_{up} = 55 \Omega m$.

Deleted: regularization constraints between neighboring nodes are set to a factor of

Deleted: , while the horizontal

Deleted: regularization

Deleted: is set to a

513 To create the final regular 3D CF-model the Ψ_{res} values from the geophysical models, the Ψ_{log} values
514 from the boreholes, and associated variances are used in a 2D-kriging interpolation for each calculation
515 interval. The 2D-grids are then stacked to form the 3D-CF-model. The Ψ_{log} values are primarily used to
516 close gaps in the resistivity dataset where boreholes are present, as seen for the large central hole in the
517 resistivity survey (Figure 8b), which is partly closed in the CF-model domain (Figure 8d) by borehole
518 information. In order to match the computational grid setup of a subsequent groundwater model, a
519 horizontal discretization of 100 m is used for the 3D-CF-model grid. In this case the dense EM-airborne
520 survey data could actually support a finer horizontal discretization (25-50 m) in the CF-model.

Deleted: The Sstarting model and the constraints setup are based on a visual comparison of the resistivity models compared to key lithological logs combined with experience and the expected geological variability and fine-tuned through a subsequent of test-inversions.

Deleted: Node points in the translator function grid situated in major data gaps (above terrain, below DOI of the resistivity models, and outside geophysical coverage) dose not come in to play at all, and are only included to made the translator function grid regular for easier computation/bookkeeping. are purely driven by the model constraints and the starting model. The effective number of translator functions, that are situated in the vicinity of resistivity models and borehole data is are therefore approximately 5,200

521 The k-means clustering is performed on two variables, the CT-model and resistivity model, in a 3D grid
522 with regular horizontal discretization of 100 m and vertical discretization of 4 m between 96 and 0 masl
523 and 8 m between 0 and 120 mbsl. CF-model values range between 0 and 1 and have therefore not been
524 standardized. The resistivity values have been log transformed and standardized by first subtracting the

Deleted: In the interpolation to make the regular 3D CF-model, Ψ_{log} values are included together with the Ψ_{res} values

555 mean and then dividing by four times the standard deviation. The standardization of the resistivity was
556 performed in this way to balance the weight between the two variables in the clustering. A five cluster
557 delineation is presented for the Norsminde case in the result section.

558 4.4 Results

559 CF-modeling results from the Norsminde area are presented in cross sections in [Figure 7](#) and as
560 horizontal slices in [Figure 8](#). [The total misfit of equation \(7\) is 0.37, but probably more interesting the](#)
561 [isolated data fit \(equation \(3\)\) is 1.26 meaning that we fit the data almost to the level of the assigned](#)
562 [noise. Figure 7a and b show the inversion results of the \$m_{low}\$ and \$m_{up}\$ parameters in section view. The](#)
563 [vertical variation in the translator is pronounced in the resistivity transition zones, because sharp layer](#)
564 [boundaries have a smoother representation in the resistivity domain.](#)

565 [For the deeper part of the model \(below elevation -10 m\) the translator functions are less varying. This](#)
566 [corresponds well to the general geological setting of the area with relatively homogenous clay sequences](#)
567 [in the deeper part, but it is also a result of very limited borehole information for the deeper model parts.](#)

568 The general geological setting of the area is also clearly reflected in the translator function in the
569 horizontal slices in [Figure 8a](#) and b. The eastern part of the area with lowest m_{low} values (dark blue in
570 [Figure 8a](#)) and lowest m_{up} values (light blue/green in [Figure 8b](#)) corresponds to the area where the
571 Palaeogene highly conductive clays are present. In the western part of the area the cross section intersect
572 the glacial complex, where the clays are mostly tills, and higher m_{low} and m_{up} values are needed to get the
573 optimum translation.

574 The resistivity cross section in [Figure 7c](#) and the slice section in [Figure 8c](#) reveal a detailed picture of the
575 effect of the geological structures seen in the resistivity data. Generally, a good correlation [with the](#)
576 [boreholes](#) is observed. Translating the resistivities we obtain the CF-model presented in [Figure 7d](#) and
577 [Figure 8d](#). The majority of the voxels in the CF-model have values close to 0 or 1. This is expected since
578 the lithological logs are described binary clay/non clay, and Ψ_{log} values not equal to 0 or 1 can only occur
579 [if both clay and non-clay lithologies are present in the same calculation interval in a particular borehole.](#)

580 Evaluating the result in [Figure 7d](#) and [Figure 8d](#), it is obvious that the very resistive zones are translated
581 to a CF-value close to 0 and the very conductive zones are translated to CF-value close to 1. Focusing on
582 the intermediate resistivities (20-60 Ω m) it is clear that the translation of resistivity to CF is not one-to-
583 one. For example, the buried valley structure (profile coordinate 6500-8500m, [Figure 7d](#)) has mostly
584 high-resistive fill with some intermediate resistivity zones. In the CF-section these intermediate resistivity
585 zones are translated to zones of high clay content, consistent with the lithological log at profile coordinate
586 7,000 m that contains a 25 m thick clay layer. The CF-section sharpens the layer boundaries compared to

Deleted: and discussion

Deleted: The variations in the translator function are relatively smooth, especially in the

Deleted:

Deleted: . The smooth

Deleted: for the deeper part

Deleted: due to

Deleted: ¶
Beside the regularization and initial starting model two main parts control the resulting m_{low} og m_{up} . The first part concerns the fact that both units described as clay and non-clay in the lithological logs can exhibit a relatively wide range of resistivities. For example, heavy clays may have resistivities of 2-3 Ω m and firm and dry clay tills can have relatively high resistivities in the range of 80 Ω m. Furthermore, changes in resistivity occur within the same geological unit due to changes in the pore water resistivity as described by Archie's law. The second issue concerns the resolution of the true formation resistivity in the resistivity models. Lithological logs contain point information with a good and uniform vertical resolution. Contrary, AEM data provide a good spatial coverage, but the vertical resolution for the EM resistivity models is relatively poor and not necessarily returning the true resistivity of the formation. Especially thin high-resistivity layers (sand layers) at great depth are poorly resolved by the EM-methods making geological interpretation difficult. By allowing spatial variation in the translator function we can, to some degree, resolve weak layer indications in the resistivity models lithologically correct while also accounting for variations in the pore water resistivity and other resistivity changes within the same lithological description.

Deleted: to

Deleted: if more

Deleted: cal

Deleted: layers

Deleted:

635 the smooth layer transitions in the resistivity section. The integration of the resistivity data and
636 lithological logs in the CF-concepts results in a high degree of consistency between the CF-results and the
637 lithological logs, as seen in the CF-section in [Figure 7d](#).

638 Horizontal slices of the 3D cluster model are shown in [Figure 9](#). The near-surface part of the model
639 ([Figure 9a-b](#)) are dominated by clusters 2 and 4, while the deeper parts of the model ([Figure 9c-d](#)) are
640 dominated by clusters 3 and 5, with the east-west striking buried valley to the south, ([Figure 9c](#)), is
641 primarily represented by clusters 1 and 2.

642 The histograms in [Figure 10](#) show how the original variables, the CF-model and the resistivity model, are
643 represented in the five clusters. Clusters 3 and 5 have resistivity values almost exclusively below 10 Ωm
644 and CF values above 0.7, but mostly close to 1. In the resistivity model space clusters 2 and 4 represent
645 high and intermediate resistivity values respectively with some overlap, while cluster 1 overlap both
646 clusters 2 and 4. [Figure 10](#) also clearly shows that both the resistivity values and the CF-values contribute
647 to the final clusters. The clusters 1, 2, and 4 span only part of the resistivity space with significant
648 overlaps ([Figure 10a](#)), while they are clearly separated in the CF-model space and spanning the entire
649 interval ([Figure 10b](#)). The opposite is observed for clusters 3, 4, and 5, which are clearly separated in the
650 resistivity space ([Figure 10a](#)), but strongly overlapping in the CF-model space ([Figure 10b](#)).

651 The CF-model does not differentiate between clay types, contrary the EM-resistivity data that have a
652 good resolution in the low resistivity range and therefore, to some degree, are able to distinguish between
653 clay types. This results in the two-part clustering of the low resistivity ($>20 \Omega\text{m}$) values as seen in ([Figure](#)
654 [10a](#)).

655 **5 DISCUSSION**

656 **5.1 Translator function, grid and discretization**

657 The spatially varying resistivity to CF translator function is the key to achieve consistency between the
658 borehole information and the resistivity models, and the spatial variations of the translator model accounts
659 for, at least, two main phenomena: 1) Changes in the resistivity-lithology petrophysical relationship, 2)
660 The resolution capability in the geophysical results.

661 The first issue includes spatial changes in; the pore water resistivity, the degree of water saturation, and/or
662 contents of clay minerals for the sediments described lithologically as clay. The spatial variation in the
663 pore water resistivity on this modeling scale is probably relatively smooth and small and will therefore
664 only have a minor impact on the resistivity to lithology/clay fraction translation. Though, in the case of

Deleted: ¶

The CF-model does not differentiate between clay types, contrary the EM-resistivity data that have a good resolution in the low resistivity range and therefore, to some degree, distinguish between clay types. This results in the two-part clustering of the low resistivity ($>20 \Omega\text{m}$) values as seen in ([Figure 9](#)[Figure 9a](#)).¶

674 saline pore water, the pore water resistivity needs to be taken into account in the interpretation. This is
675 particularly important in the (rare) case where the presence of saline pore water might violate the basic
676 assumption that clay rich formations are more conductive than coarse-grained sediments.

677 The varying content of clay minerals in the lithologies described as *clay* will effect the translator model.
678 The correlation between the clay mineral content and resistivity is quite strong and could be the key
679 parameter instead of the simple clay fraction of this concept, but it would require clay mineral content
680 values available in boreholes on a large modeling scale, which is why we disregard this approach and use
681 the intentionally simple definition of clay and clay fraction.

682 The second issue concerns the resolution of the true formation resistivity in the resistivity models.
683 Lithological logs contain point information with a good and uniform vertical resolution. Contrary, AEM
684 data provide a good spatial coverage, but the vertical resolution is relatively poor and decreasing with
685 depth. Detailed geological layer sequences might only be represented by an average conductivity or only
686 have a weak signature in the resistivity models. By allowing spatial variation in the translation we can, to
687 some degree, resolve weak layer indications in the resistivity models by utilizing the vertically detailed
688 structural information from the lithological logs via the translator function.

689 The horizontal sampling of the translator function should in principle be able to reproduce the true (but
690 unknown) variations in the resistivity to CF translation. Though, it is primarily the borehole density and
691 secondarily the complexity of the petrophysical relationship between clay and resistivity, that dictates the
692 needed horizontal sampling of the translator function. To our experience a horizontal discretization of the
693 translator function grid of 1-2 km (linearly interpolated between nodes) is sufficient to obtain an
694 acceptable consistency between the lithological logs and the translated resistivities. For the deeper part of
695 the model domain where the borehole information is sparse, a coarser translator function grid would be
696 sufficient.

697 Starting model values for the translator function in the inversion scheme becomes important in areas with
698 very low borehole density, primarily the deeper part of the model domain. The starting model values are
699 selected based on experience and by a visual comparison of the resistivity models to key lithological logs.
700 The horizontal and vertical constraints to migrate some information from regions with many boreholes to
701 regions with few boreholes or with no boreholes. As in most inversion tasks a few initial inversions are
702 performed to fine-tune and to evaluate the effect of different starting models and constraints setup.

703 The CF-concept supports both uncertainty estimates on the input data, on the output translator functions,
704 and on the final CF-model. Generally, the uncertainties in the CF-model are closely related to the
705 borehole density and quality, as well as resolution and density of the resistivity models. The calculation
706 and estimation of input and output uncertainties is described in detail in Christiansen et al. (2014).

707 **5.2 Clustering and validation**

708 For the clustered 3D-model each cluster represent some unit with fairly uniform characteristics. It could
709 be hydrostratigraphic units where the hydraulic conductivity of the cluster units are determined through a
710 subsequent groundwater model calibration, typically constrained by hydrological head and discharge data.
711 Groundwater model calibration of the Norsminde 3D-cluster model has been performed with a
712 preliminary positive outcome, but more experiments are needed before drawing final conclusions. In this
713 process one needs to evaluate the cluster validity, i.e. how many clusters the data can support. Cluster
714 validity can be assessed with various statistical measures (e.g. Halkidi et al., 2002). The number of
715 clusters resulting in the best hydrological performance might also be used as a measure of cluster validity.
716 The validity of the clusters and the resulting groundwater model is still to be explored in more detail.

717 **6 CONCLUSION**

718 We have presented a concept to produce 3D clay-fraction models, integrating the key sources of
719 information in a well-documented and objective way.

720 The concept combines lithological borehole information with geophysical resistivity models in producing
721 large scale 3D clay fraction models. The integration of the lithological borehole data and the resistivity
722 models is accomplished through inversion, where the optimum resistivity to clay fraction function
723 minimizes the difference between the observed clay fraction from boreholes and the clay fraction found
724 through the geophysical resistivity models. The inversion concept allows for horizontal and lateral
725 variation in the resistivity to clay fraction translation, with smoothness constraints as regularization. The
726 spatially varying translator function is the key to achieve consistency between the borehole information
727 and the resistivity models. The concept furthermore handles uncertainties on both input and output data.

728 The concept was applied to a 156 km² survey with more than 700 boreholes and 100,000 resistivity
729 models from an airborne survey. The output was a detailed 3D clay fraction model combining resistivity
730 models and lithological borehole information into one parameter.

731 Finally a cluster analysis was applied to achieve a predefined number of geological/hydrostratigraphic
732 clusters in the 3D-model and enabled us to integrate various sources of information, geological as well as
733 geophysical. The final five-cluster model differentiates between clay materials and different high resistive
734 materials from information held in resistivity model and borehole observations respectively.

735 With the CF-concept and clustering we aim at building 3D models suitable as structural input for
736 groundwater models. Each cluster will then represent a hydrostratigraphic unit and the hydraulic

Deleted: AND OUTLOOK

738 conductivity of the units will be determined through the groundwater model calibration constrained by
739 hydrological head and discharge data.

740 The 3D clay fraction model can also be seen as a binomial geological sand-clay model by interpreting
741 the high and low CF-values as clay and sand respectively, as the color scale for the CF-model example in
742 [Figure 7](#) and [Figure 8](#) indicated. Integration and further development of the CF-model into more complex
743 geological models have been carried out with success ([Jørgensen et al., 2013b](#)).

Deleted: For the case study, we have not evaluated cluster validity, i.e. how many clusters the data can support. Cluster validity can be assessed with various statistical measures (Halkidi et al., 2002). If the cluster model is used as structural input to a groundwater model the number of clusters resulting in the best hydrological performance (keeping in mind the principle of parsimony) might also be used as a measure of cluster validity.

Deleted: (Jørgensen et al., 2013c)

744 **7 ACKNOWLEDGEMENTS**

745 The research for this paper was carried out within the STAIR3D-project (funded by Geo-Center
746 Danmark) and the HyGEM-project (funded by the Danish Council for Strategic Research under contract
747 no. DSF 11-116763). We also wish to thank the NiCA research project (funded by the Danish Council
748 for Strategic Research under contract no. DSF 09-067260) for granting access to the SkyTEM data for the
749 Norsminde case and senior advisor at the Geological Survey of Denmark and Greenland (GEUS), Claus
750 Ditlefsen, for his work and help with quality rating of the borehole data. Finally a great thanks to our
751 colleagues, Ph.D. Casper Kirkegaard for help with optimization of the numerical code and Professor
752 emeritus Niels Bøje Christensen for insightful comments on the uncertainty migration.

753 **REFERENCES**

754 [Auken, E. and A. V. Christiansen, 2004, Layered and laterally constrained 2D inversion of resistivity
755 data: *Geophysics*, 69, 3, 752-761.](#)

756 [Auken, E., A. V. Christiansen, B. H. Jacobsen, N. Foged, and K. I. Sørensen, 2005, Piecewise 1D
757 Laterally Constrained Inversion of resistivity data: *Geophysical Prospecting*, 53, 497-506.](#)

758 [Auken, E., A. V. Christiansen, C. Kirkegaard, G. Fiandaca, C. Schamper, A. A. Behroozmand, A. Binley,
759 E. Nielsen, F. Effersø, N. B. Christensen, K. I. Sørensen, N. Foged, and G. Vignoli, 2014, An overview of
760 a highly versatile forward and stable inverse algorithm for airborne, ground-based and borehole electric
761 and electromagnetic data: *Exploration Geophysics*, **Submitted**.](#)

762 [Auken, E., A. V. Christiansen, J. A. Westergaard, C. Kirkegaard, N. Foged, and A. Viezzoli, 2009, An
763 integrated processing scheme for high-resolution airborne electromagnetic surveys, the SkyTEM system:
764 *Exploration Geophysics*, 40, 184-192.](#)

765 [Bussian, A. E., 1983, Electrical conductance in a porous medium: *Geophysics*, 48, 9, 1258-1268.](#)

766 [Christiansen, A. V. and E. Auken, 2012, A global measure for depth of investigation: *Geophysics*, 77, 4,
767 WB171-WB177.](#)

780 [Christiansen, A. V., N. Foged, and E. Auken, 2014, A concept for calculating accumulated clay thickness](#)
781 [from borehole lithological logs and resistivity models for nitrate vulnerability assessment: Journal of](#)
782 [Applied Geophysics, Revised version submitted.](#)

783 [Clavier, C., G. Coates, and J. Dumanoir, 1984, Theoretical and experimental bases for the dual-water](#)
784 [model for interpretation of shaly sands: Society of Petroleum Engineers Journal, 24, 2, 153-168.](#)

785 [Daly, C. and J. K. Caers, 2010, Multi-point geostatistics - an introductory overview: First Break, 28, 9,](#)
786 [39-47.](#)

787 [Dam, D. and S. Christensen, 2003, Including geophysical data in ground water model inverse calibration:](#)
788 [Ground Water, 41, 2, 178-189.](#)

789 [Deutsch, C. V. and A. G. Journel, 1998, GSLIB: geostatistical software library and user's guide. Second](#)
790 [edition: Oxford University Press.](#)

791 [Fogg, G. E., 1996, Transition Probability-Based Indicator Geostatistics: Mathematical Geology, 28, 4,](#)
792 [453-476.](#)

793 [Geonics Limited, 2012, http://www.geonics.com/index.html:](#)

794 [Härdle, K. W. and L. Simar, 2012, Applied Multivariate Statistical Analysis: Springer.](#)

795 [He, X., J. Koch, T. O. Sonnenborg, F. Jørgensen, C. Schamper, and J. C. Refsgaard, 2014, Transition](#)
796 [probability based stochastic geological modeling using airborne geophysical data and borehole data:](#)
797 [Water Resources Research, Special Issue on Patterns in Soil-Vegetation-Atmosphere Systems:](#)
798 [Monitoring, Modeling and Data Assimilation, 1-23.](#)

799 [Herckenrath, D., G. Fiandaca, E. Auken, and P. Bauer-Gottwein, 2013, Sequential and joint](#)
800 [hydrogeophysical inversion using a field-scale groundwater model with ERT and TDEM data: Hydrology](#)
801 [and Earth System Sciences, 17, 4043-4060.](#)

802 [Hinnell, A. C., T. P. A. Ferre, J. A. Vrugt, J. A. Huisman, S. Moysey, J. Rings, and M. B. Kowalsky,](#)
803 [2010, Improved extraction of hydrologic information from geophysical data through coupled](#)
804 [hydrogeophysical inversion: Water Resources Research, 46, 4, DOI: 10.1029/2008WR007060.](#)

805 [Hotelling, H., 1933, Analysis of a complex of statistical variables into principal components: Journal of](#)
806 [Educational Psychology, 24, 417-441.](#)

807 [Høyer, A.-S., F. Jørgensen, H. Lykke-Andersen, and A. V. Christiansen, 2014, Iterative modelling of](#)
808 [AEM data based on geological a priori information from seismic and borehole data: Near Surface](#)
809 [Geophysics, 12,](#)

810 [Jørgensen, F., R. R. Møller, L. Nebel, N. Jensen, A. V. Christiansen, and P. Sandersen, 2013a, A method](#)
811 [for cognitive 3D geological voxel modelling of AEM data: Bulletin of Engineering Geology and the](#)
812 [Environment, 72, 3-4, 421-432, DOI: 10.1007/s10064-013-0487-2.](#)

813 [Jørgensen, F. and P. B. E. Sandersen, 2006, Buried and open tunnel valleys in Denmark-erosion beneath](#)
814 [multiple ice sheets: Quaternary Science Reviews, 25, 11-12, 1339-1363.](#)

815 [Jørgensen, F., P. B. E. Sandersen, A.-S. Høyer, T. M. Pallesen, N. Foged, X. He, and T. O. Sonnenborg,](#)
816 [2013b, A 3D geological model from Jutland, Denmark: Combining modeling techniques to address](#)

817 [variations in data density, data type, and geology: Denver, Colorado, USA, 125th Anniversary Annual](#)
818 [Meeting](#)

819 [Jørgensen, F., W. Scheer, S. Thomsen, T. O. Sonnenborg, K. Hinsby, H. Wiederhold, C. Schamper,](#)
820 [Roth.B., R. Kirsch, and E. Auken, 2012, Transboundary geophysical mapping of geological elements](#)
821 [and salinity distribution critical for the assessment of future sea water intrusion in response to sea level](#)
822 [rise: Hydrology and Earth System Sciences, 16, 1845-1962.](#)

823 [Paasche, H., J. Tronicke, K. Holliger, A. G. Green, and H. Maurer, 2006, Integration of diverse physical-](#)
824 [property models: Subsurface zonation and petrophysical parameter estimation based on fuzzy c-means](#)
825 [cluster analyses: Geophysics, 71, H33-H44.](#)

826 [Pebesma, E. J. and C. G. Wesseling, 1998, Gstat: A Program for geostatistical Modelling, Prediction and](#)
827 [Simulation: Computers & Geosciences, 24, 1, 17-31.](#)

828 [Raiber, M., P. A. White, C. J. Daughney, C. Tschirter, P. Davidson, and S. E. Bainbridge, 2012, Three-](#)
829 [dimensional geological modelling and multivariate statistical analysis of water chemistry data to analyse](#)
830 [and visualise aquifer structure and groundwater composition in the Wairau Plain, Marlborough District,](#)
831 [New Zealand: Journal of Hydrology, 436-437, 13-34.](#)

832 [Refsgaard, A., E. Auken, C. A. Bamberg, B. S. B. Christensen, T. Clausen, E. Dalgaard, F. Effersø, V.](#)
833 [Ernstsen, F. Gertz, A. L. Hansen, X. He, B. H. Jacobsen, K. H. Jensen, F. Jørgensen, L. F. Jørgensen, J.](#)
834 [Koch, B. Nilsson, C. Petersen, G. DeSchepper, C. Schamper, K. I. Sørensen, R. Therrien, C. Thirup, and](#)
835 [A. Viezzoli, 2014, Nitrate reduction in geologically heterogeneous catchments - A framework for](#)
836 [assessing the scale of predictive capability of hydrological models: ScienceDirect, 468-469, 1278-1288.](#)

837 [Revil, A. and P. W. J. Glover, 1998, Nature of surface electrical conductivity in natural sands, sandstones,](#)
838 [and clays: Geophysical Research Letters, 25, 5, 691-694.](#)

839 [Sandersen, P., F. Jørgensen, N. K. Larsen, J. H. Westergaard, and E. Auken, 2009, Rapid tunnel-valley](#)
840 [formation beneath the receding Late Weichselian ice sheet in Vendsyssel, Denmark: BOREAS, 38, 4,](#)
841 [834-851, DOI: 10.1111/j.1502-3885.2009.00105.x.](#)

842 [Schamper, C., E. Auken, and K. I. Sørensen, 2014, Coil response inversion for very early time modeling](#)
843 [of helicopter-borne time-domain EM data and mapping of near-surface geological layers: Geophysical](#)
844 [Prospecting, In press.](#)

845 [Schamper, C., F. Jørgensen, E. Auken, and F. Effersø, 2013, Resolution of thin and shallow geological](#)
846 [layers using airborne transient electromagnetics: Geophysics, submitted.](#)

847 [Seifert, D., T. O. Sonnenborg, J. C. Refsgaard, A. L. Højberg, and L. Troldborg, 2012, Assessment of](#)
848 [hydrological model predictive ability given multiple conceptual geological models: Water Resources](#)
849 [Research, 48, 6, DOI: 10.1029/2011WR011149.](#)

850 [Sen, P. N., 1987, Electrochemical origin of conduction in shaly formations: Society of Petroleum](#)
851 [Engineers: Presented at 62nd Annual Technical Conference and Exhibition.](#)

852 [Slater, L., 2007, Near surface electrical characterization of hydraulic conductivity: From petrophysical](#)
853 [properties to aquifer geometries - A review: Surveys in Geophysics, 28, 2-3, 169-197.](#)

854 [Stafleu, J., D. Maljers, J. L. Gunnink, A. Menkovic, and F. S. Busschers, 2011, 3D modelling of the](#)
855 [shallow subsurface of Zeeland, the Netherlands: Geologie en Mijnbouw/Netherlands Journal of](#)
856 [Geosciences, 90, 4, 293-310.](#)

857 [Strebelle, S., 2002, Conditional simulation of complex geological structures using multiple-point](#)
858 [statistics: Mathematical Geology, 34, 1, 1-21.](#)

859 [Triantafylis, J. and S. M. Buchanan, 2009, Identifying common near-surface and subsurface stratigraphic](#)
860 [units using EM34 signal data and fuzzy k-means analysis in the Darling River valley: Australian Journal](#)
861 [of Earth Sciences, 56, 535-558.](#)

862 [Turner, A., 4-5-2006, Challenges and trends for geological modelling and visualisation: Bulletin of](#)
863 [Engineering Geology and the Environment, 65, 2, 109-127.](#)

864 [Viezzoli, A., A. V. Christiansen, E. Auken, and K. I. Sørensen, 2008, Quasi-3D modeling of airborne](#)
865 [TEM data by Spatially Constrained Inversion: Geophysics, 73, 3, F105-F113.](#)

866 [Waxman, M. H. and L. J. M. Smits, 1968, Electrical Conductivities in Oil-Bearing Shaly Sands: Society](#)
867 [of Petroleum Engineers Journal, 8, 107-122.](#)

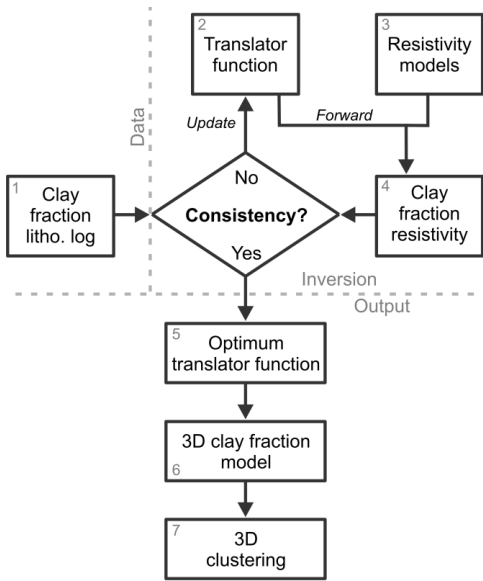
868 [Wisén, R., E. Auken, and T. Dahlin, 2005, Combination of 1D laterally constrained inversion and 2D](#)
869 [smooth inversion of resistivity data with a priori data from boreholes: Near Surface Geophysics, 3, 71-79.](#)

870 [Wu, j., 2012, Advances in K-means Clustering: A Data Mining Thinking: Springer.](#)
871
872
873

874 **FIGURES AND FIGURE CAPTIONS**

875 **Figure 1**

876



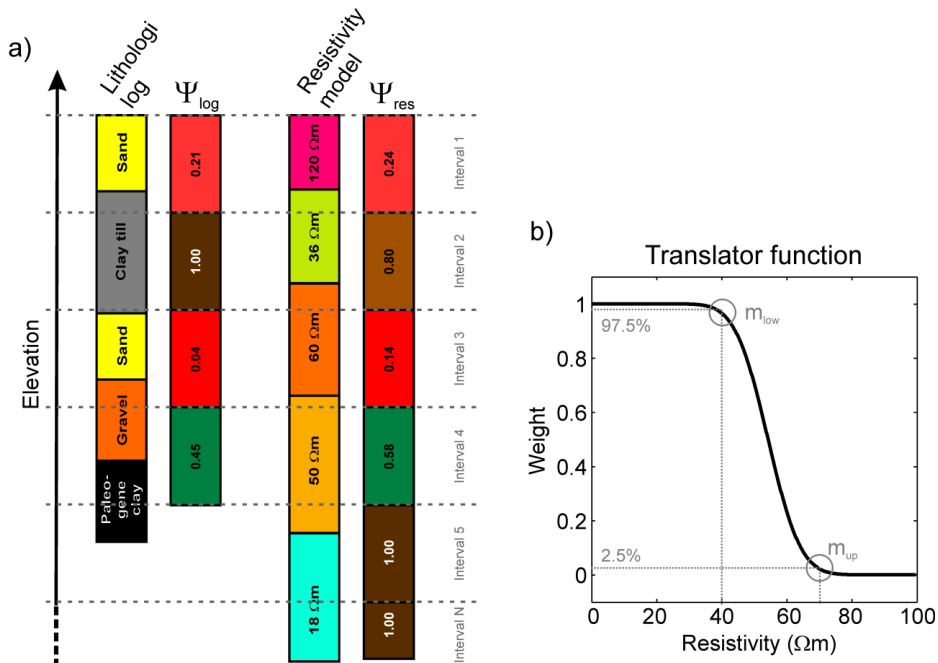
877

878 | Figure 1. Conceptual flowchart for the clay fraction concept and clustering.

879

880

Figure 2



881

882 Figure 2. a) Example on how a lithological log is translated into Ψ_{log} and how a resistivity model
 883 translates into Ψ_{res} , for a numbers of calculation intervals. The resistivity values and the resulting clay
 884 fraction values are stated on the bars, but also indicated with colors with reference to the color scales of
 885 Figure 7. b) The translator function returns a weight, W, between 0 and 1 for a given resistivity value. The
 886 translator function is defined by the two parameters m_{low} , and m_{up} . In this example the m_{low} , and m_{up}
 887 parameters are 40 Ωm and 70 Ωm respectively.

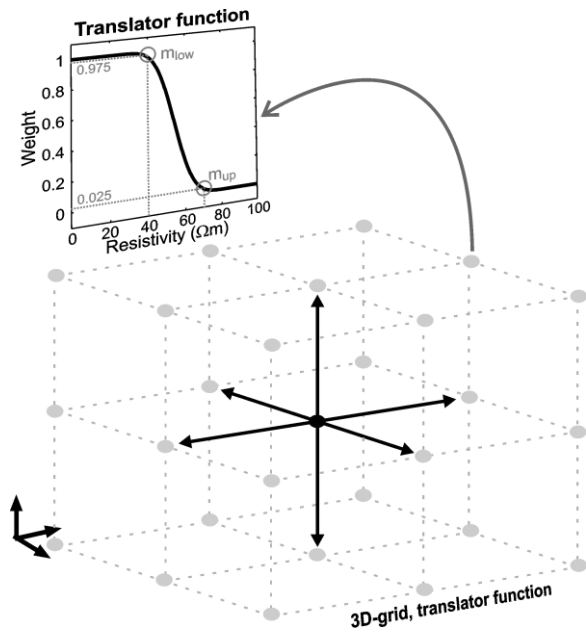
888

Moved (insertion) [1]

Deleted: The translator function returns a weight, W, between 0 and 1 for a given resistivity value. The translator function is defined by the two parameters m_{low} , and m_{up} . In this example the m_{low} , and m_{up} parameters correspond to 40 Ωm and 70 Ωm respectively

896 | **Figure 3.**

897



898

899 | **Figure 3.** The translator function and 3D translator function grid. Each node in the 3D translator function
900 grid holds a set of m_{up} and m_{low} . The m_{up} and m_{low} parameters are constrained to all neighboring
901 parameters as indicated with the black arrows for the black center node.

Deleted: 2

Deleted: 32

Moved up [1]: The translator function returns a weight, W , between 0 and 1 for a given resistivity value. The translator function is defined by the two parameters m_{low} , and m_{up} . In this example the m_{low} , and m_{up} parameters correspond to 40 Ωm and 70 Ωm respectively

Deleted: .

912

Figure 4

Deleted: 3

913



914

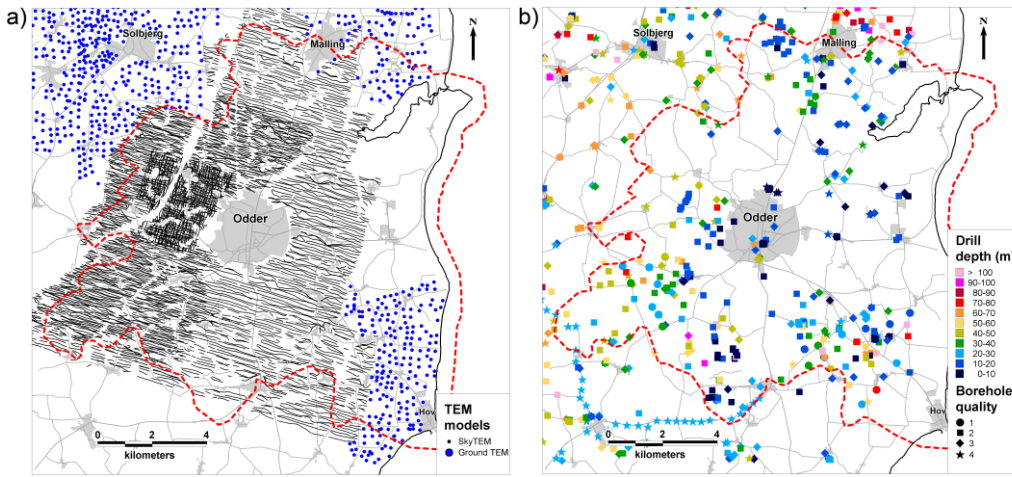
915

Figure 4. The black square marks the Norsminde survey area.

Deleted: 43

918

Figure 5



Deleted: 4

919

920 Figure 5. a) Resistivity model positions for the SkyTEM survey and the ground-based TEM soundings.
 921 b) Borehole locations, quality (shape), and drill depth (color). Quality 1 corresponds to the highest
 922 quality and 4 to the lowest quality. The red dashed line outlines the catchment area (156 km²).

Deleted: 54

Deleted: Location of the r

Deleted: s

Deleted: s

Deleted: . Small dots are

Deleted: models, larger scattered dots

Deleted: are

Deleted: models

Deleted: and borehole

Deleted: where

Deleted: modeling area

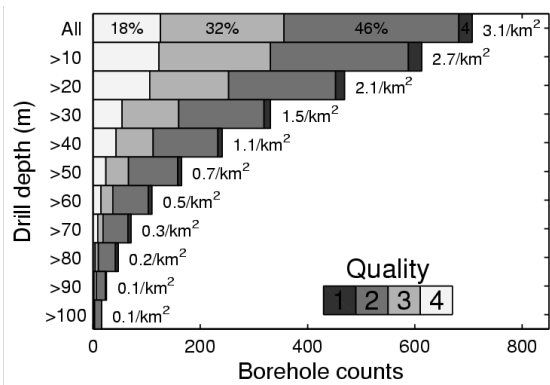
Deleted: 5

923

924

Figure 6

925



926

927 Figure 6. Number of boreholes vs. drill depth. The bars show how many boreholes reach a certain depth.
 928 The value to the right of the bars state the number of boreholes per km² for minimum depth of the
 929 interval. The color coding of the bars marks the quality grouping.

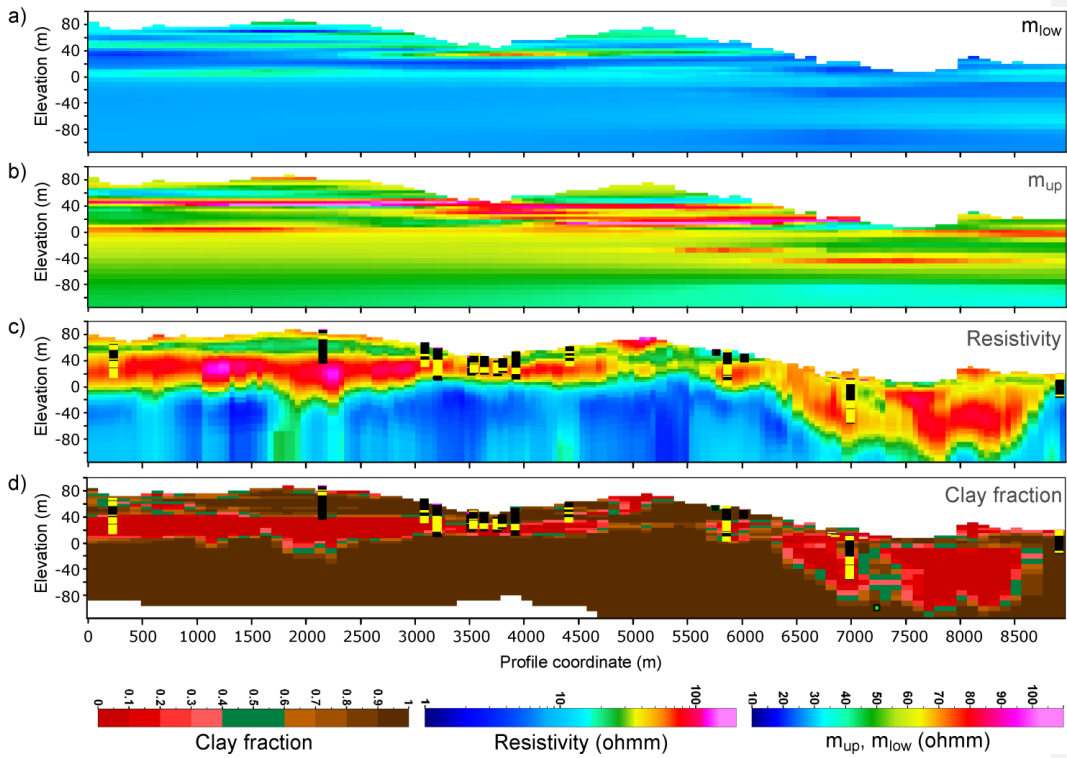
Deleted: 65

944

Figure 7

945

Deleted: Page Break
F



946

947 Figure 7 Northwest-southeast cross sections (vertical exaggeration x6). Location and orientation of cross
 948 sections are marked in Figure 8. a) The m_{low} parameters of the translator function. b) The m_{up} parameters
 949 of the translator function. c) The resistivity section with boreholes within 200 m of the profile
 950 superimposed. Black borehole colors mark the clay layers, while yellow colors mark sand and gravel
 951 layers. d) Clay fraction section and boreholes (same as plotted in the resistivity section).

952

Deleted: 76

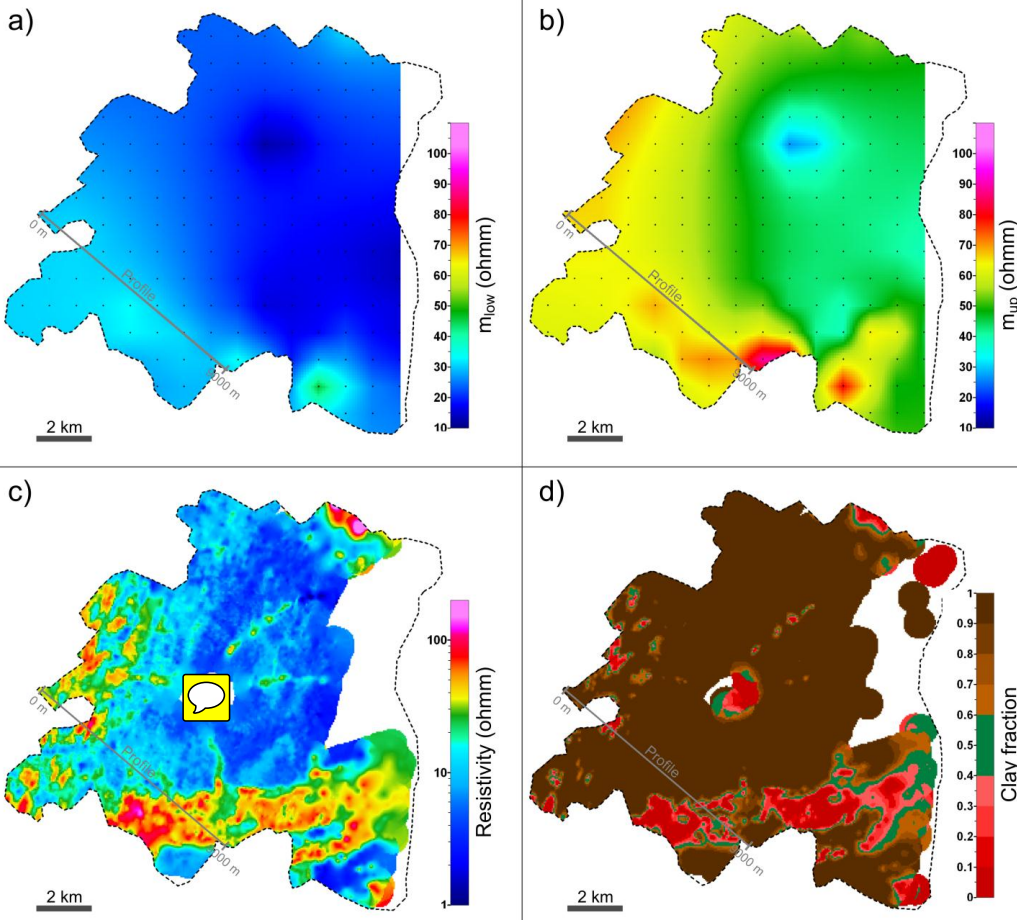
Deleted: Figure 8Figure 7

958

Figure 8

Deleted: 7

959



960

961 | Figure 8. Horizontal slices at 2 mbsl cropped to the catchment area (dashed line). a) The m_{low} parameters
 962 | of the translator function superimposed with the 1 km translator function grid (black dots). b) The m_{up}
 963 | parameters of the translator function superimposed with the 1 km translator function grid (black dots). c)
 964 | Resistivity slice (interpolated). d) Resulting CF- model.

Deleted: 87

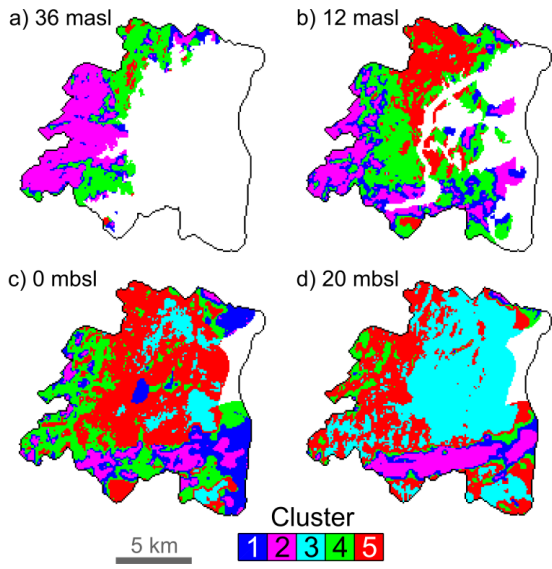
Deleted: Interpolated r

968

Figure 9.

Deleted: 8

969



970

971 | Figure 9. Horizontal slices in four depths of the 3D cluster model.

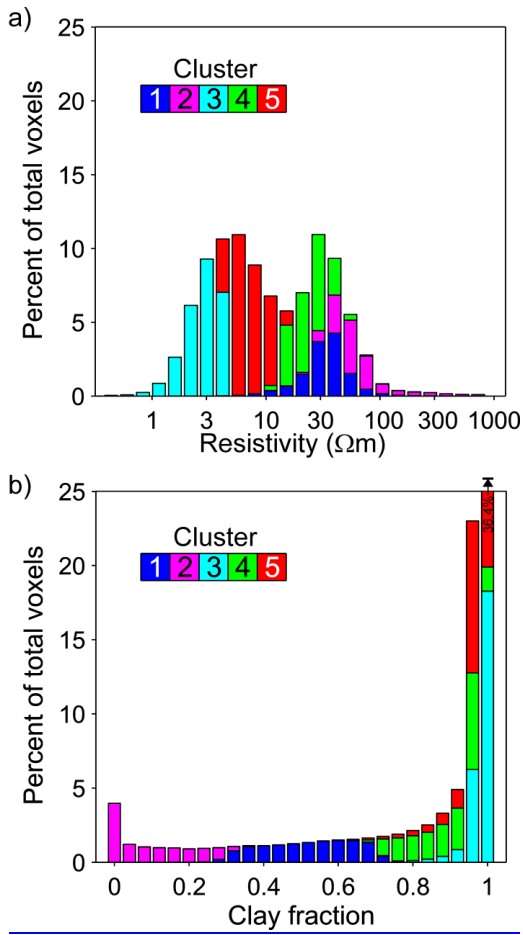
Deleted: 98

974

Figure 10

Deleted: 9

975



976

977

Figure 10. Cluster statistics. The histograms show which data from the original variables make up the five clusters. a) The distribution of the resistivity data in the five clusters. b) The distribution of the CF data in the five clusters.

Deleted: 109

979